Available online at www.sciencedirect.com
SCIENCE DIRECT®
Remote Sensing of Environment 85 (2003) 429–440
Remote Sensing of Environment
www.elsevier.com/locate/rse

Estimating subpixel surface temperatures and energy fluxes from the vegetation index–radiometric temperature relationship

William P. Kustas[a,*], John M. Norman[b], Martha C. Anderson[b], Andrew N. French[c]

[a] Hydrology and Remote Sensing Laboratory, USDA-ARS, Building 007, BARC West, Room 104, Beltsville, MD 20705-2350, USA
[b] Department of Soil Science, University of Wisconsin, Madison, WI, USA
[c] Hydrological Sciences Branch, NASA Goddard, Greenbelt, MD, USA

Received 3 October 2002; received in revised form 13 January 2003; accepted 18 January 2003

Abstract

Routine (i.e., daily to weekly) monitoring of surface energy fluxes, particularly evapotranspiration (ET), using satellite observations of radiometric surface temperature has not been feasible at high pixel resolution (i.e., $\sim 10^1$–10^2 m) because of the low frequency in satellite coverage over the region of interest (i.e., approximately every 2 weeks). Cloud cover further reduces the number of useable observations of surface conditions resulting in high-resolution satellite imagery of a region typically being available once a month, which is not very useful for routine ET monitoring. Radiometric surface temperature observations at ~ 1- to 5-km pixel resolution are available multiple times per day from several weather satellites. However, this spatial resolution is too coarse for estimating ET from individual agricultural fields or for defining variations in ET due to land cover changes. Satellite data in the visible and near-infrared wavelengths, used for computing vegetation indices, are available at resolutions an order of magnitude smaller than in the thermal-infrared, and hence provide higher resolution information on vegetation cover conditions. A number of studies have exploited the relationship between vegetation indices and radiometric surface temperature for estimating model parameters used in computing spatially distributed fluxes and available moisture. In this paper, the vegetation index–radiometric surface temperature relationship is utilized in a disaggregation procedure for estimating subpixel variation in surface temperature with aircraft imagery collected over the US Southern Great Plains. The disaggregated surface temperatures estimated by this procedure are compared to actual observations at this subpixel resolution. In addition, a remote sensing-based energy balance model is used to compare output using actual versus estimated surface temperatures over a range of pixel resolutions. From these comparisons, the utility of the surface temperature disaggregation technique appears to be most useful for estimating subpixel surface temperatures at resolutions corresponding to length scales defining agricultural field boundaries across the landscape.
Published by Elsevier Science Inc.

Keywords: Subpixel surface temperature; Vegetation index; Radiometric surface

1. Introduction

Estimation of field scale (i.e., length scales $\sim 10^1$–10^2 m) evapotranspiration (ET) has been achieved using high spatial but low temporal resolution satellite data from the Land remote-sensing satellite Thematic Mapper (Landsat TM) and the Advanced Spaceborne Thermal Emission and Reflection Radiometer (ASTER) (e.g., French, Schmugge, & Kustas, 2002; Moran et al., 1996). However, given the long repeat cycle of these satellites (16 days), such methods are not well-suited for routine ET estimation. Others have used coarser resolution satellite data available on a daily or more frequent basis from the Advanced Very High Resolution Radiometer (AVHRR) and Geostationary Orbiting Environmental Satellite (GOES) in an attempt to achieve routine ET monitoring (e.g., Mecikalski, Diak, Anderson, & Norman, 1999; Seguin, Lagouarde, & Saranc, 1991). The pixel resolution of these satellites, however, is ~ 1 to 5 km, meaning that the ET estimates represent averages over areas of ~ 1 to 25 km^2. Agricultural fields in the Southern Great Plains are typically on the order of 10^2 to 10^3 hectares or 10^{-1} to 10^0 km^2 (Jackson et al., 1999); hence, the coarser pixel resolution data cannot be used to discriminate ET of individual fields.

From a more global perspective, Townshend and Justice (1988) degraded Landsat satellite imagery collected over a

* Corresponding author. Tel.: +1-301-504-8498; fax: +1-301-504-8931.
E-mail address: bkustas@hydrolab.arsusda.gov (W.P. Kustas).

0034-4257/03/$ - see front matter. Published by Elsevier Science Inc.
doi:10.1016/S0034-4257(03)00036-1

variety of landscapes to proposed pixel resolutions (250 m to 4 km) of the Moderate Resolution Imaging Spectroradiometer (MODIS) and show that for accurate assessment of land cover changes, a pixel resolution of 500 m or less is necessary. They also find that even though at the 1-km pixel resolution, land use/land cover change is detected, defining the areal extent of such changes will often be unreliable. With land use and land cover changes, there can be significant changes in surface energy balance and ET, which can be monitored with radiometric surface temperature (Kustas & Norman, 1996). However, to monitor such changes on a routine basis requires the higher temporal frequency-coarser resolution thermal-infrared data to be at the 250- to 500-m pixel size as suggested by Townshend and Justice (1988).

This deficiency can be addressed by using the functional relationship between a vegetation index and radiometric surface temperatures. This relationship has been exploited by other remote sensing-based energy balance modeling schemes for constraining/defining model variables/parameters (e.g., Carlson, Gillies, & Perry, 1994; Gillies & Carlson, 1995; Moran, Clarke, Inoue, & Vidal, 1994; Price, 1990). With a vegetation index such as the Normalized Difference Vegetation Index (NDVI), which is often available at finer pixel resolution than radiometric surface temperature (T_R), there is potential to make use of the NDVI–T_R relation to derive T_R at the NDVI pixel resolution.

A procedure for disaggregating T_R to the NDVI-pixel resolution (DisTrad) is described and evaluated using airborne remote sensing data collected during the 1997 Southern Great Plains Experiment (SGP97) conducted in Oklahoma, USA. We focus on a single day during this experiment, where there was significant heterogeneity in T_R due to large spatial variation in moisture and vegetation cover conditions across the landscape. The T_R and NDVI data are aggregated from a base resolution of 24 m to 96, 192, 768, and 1536 m. The DisTrad procedure is applied to 96- and 192-m resolution data for estimating T_R at 24 m. This represents using DisTrad with T_R observations from ASTER or Landsat TM at $\sim 10^2$-m pixel resolution and estimating T_R ($\hat{T}_R$) at the resolution of NDVI observations from these instruments, namely $\sim 10^1$ m. The DisTrad procedure is also applied to 768- and 1536-m resolution data for estimating T_R at 192 m. This represents application of DisTrad to T_R observations bracketing AVHRR and MODIS at $\sim 10^3$-m pixel resolution and estimating T_R ($\hat{T}_R$) at the NDVI pixel resolution of MODIS, namely $\sim 10^2$ m. In Table 1, the NDVI and T_R pixel resolutions are listed for the ASTER, AVHRR, GOES, Landsat, and MODIS.

In addition, a remote sensing-based energy balance model developed to use both coarse and fine resolution remotely sensed data, called the Disaggregated Atmosphere Land Exchange Inverse (DisALEXI) model, is applied to both T_R and $\hat{T}_R$. The DisALEXI model has been used with the high temporal resolution of GOES and high spatial resolution of the airborne data collected during SGP97 for estimating heat fluxes on the 10^1–10^2 m scale without requiring any local observations (Norman et al., submitted for publication). The results of the intercomparisons in heat flux estimates using both T_R and $\hat{T}_R$ are analyzed and discussed.

Table 1
Nominal satellite pixel resolutions for normalized difference vegetation index (NDVI) and radiometric surface temperature (T_R)

Satellite	NDVI pixel resolution (m)	T_R pixel resolution (m)
ASTER	15	90
AVHRR	1100	1100
GOES	4000	4000
Landsat-5	30	120
Landsat-7	30	60
MODIS	250	1000

2. Methodology

2.1. Disaggregation procedure for radiometric surface temperature (DisTrad)

The DisTrad technique is based on fitting a least-squares expression between NDVI (the dependent variable) and radiometric temperature (the independent variable) after NDVI has been aggregated to the coarser T_R resolution. To more clearly illustrate the DisTrad approach, the procedure is used to disaggregate T_R from 96- to 24-m pixel resolution.

The first step is to select a subset of pixels from the scene where NDVI is most uniform within the 96-m aggregated pixels. By using the original 24-m resolution NDVI data ($NDVI_{24}$), the coefficient of variation (CV, the standard deviation divided by the mean) is computed among the 4×4 pixels (16 pixels in total) that make up each 96-m NDVI pixel, ($NDVI_{96}$). The $NDVI_{96}$ pixels are divided into several groups/classes, namely, $0 < NDVI_{96} < 0.2$ (sparse canopy cover/bare soil), $0.2 < NDVI_{96} < 0.5$ (partial canopy cover) and $NDVI_{96} > 0.5$ (high/full canopy cover); then a fraction ($\sim 1/4$) of pixels having the lowest CV are selected from each class. By isolating pixels with relatively uniform cover at the 96-m scale, the relation derived between T_R and NDVI at 96 m should more closely resemble the relations at higher resolutions. Moreover, subsetting by cover class promotes higher dynamic range in the resulting T_R–NDVI distributions.

Next, a least-squares fit is performed relating T_{R96} and $NDVI_{96}$ values associated with this subset of "uniform" pixels using the following expression:

$$\hat{T}_{R96}(NDVI_{96}) = a + bNDVI_{96} + cNDVI_{96}^2 \quad (1)$$

A linear equation ($c = 0$) between T_{R96} and $NDVI_{96}$ may be more suitable in some cases, particularly when the range in

T_{R96} and $NDVI_{96}$ values is limited. In principle, Eq. (1) could be used to estimate 24-m T_R, $\hat{T}_{R24}$, directly by replacing $NDVI_{96}$ with $NDVI_{24}$. However, this would neglect effects of variations in soil moisture across the image scene because the least-squares regression, by definition, reflects only average conditions.

Spatial variability due to soil moisture effects can be incorporated into the sharpened thermal image by adjusting each 24-m pixel by the deviation from the regressed temperature observed at 96 m:

$$\Delta\hat{T}_{R96} = T_{R96} - \hat{T}_{R96} \quad (2)$$

Then, for each ith 24-m pixel within the 96-m pixel (where $i = 1,2,3\ldots16$), $\hat{T}_{R24}$ is computed via

$$\hat{T}_{R24}(i) = \hat{T}_{R96}(NDVI_{24}(i)) + \Delta\hat{T}_{R96} \quad (3)$$

where the first term on the right-hand side is evaluated using Eq. (1) with the $NDVI_{24}$ value at that pixel, and the second term accounting for deviations from the mean is evaluated from Eq. (2).

2.2. Disaggregation of the heat fluxes using DisALEXI

Norman et al. (submitted for publication) describe in detail the DisALEXI approach using the same data set as the present study. In brief, DisALEXI is driven by ALEXI output of regional air temperature at 50 m using 5-km GOES T_R observations at two times during the morning period (nominally 1.5 and 5.5 h after local sunrise). Details of ALEXI are given in Anderson et al. (1997) and Mecikalski et al. (1999). Both ALEXI and DisALEXI make use of the two-source energy balance model described by Norman et al. (1995) and Kustas and Norman (1999). The 50-m air temperature, derived from ALEXI, is then applied in the DisALEXI scheme. The high-resolution NDVI and land use with the corresponding T_R observation is used in the two-source energy balance model to derive pixel-based aerodynamic resistances from the soil, vegetation, and atmosphere. Comparisons between DisALEXI output of the fluxes over the SGP97 region and tower-based flux observations indicate that differences are typically within measurement uncertainties, namely $\sim$ 50 W m^{-2} (Twine et al., 2000).

3. Data

Details of the SGP97 study are described by Jackson et al. (1999). There is also a description of the experiment and all measurement activities provided on the World Wide Web (http://hydrolab.arsusda.gov/sgp97/). The experimental period for SGP97 ran from mid-June to mid-July 1997. The region contains a relatively dense network of meteorological stations, the Oklahoma Mesonet (Brock et al., 1995). The wind speed observations for all Mesonet stations are also having an air temperature measurement at 9 m agl. level (agl) and air temperature at 1.5 m with some stations also having an air temperature measurement at 9 m agl. Details of the measurements and quality control of the data are described by Shafer, Fiebrich, Arndt, Fredrickson, and Hughs (2000). The remotely sensed and surface flux data used in this study come from one of the three intensively monitored experimental sites, the USDA-ARS Grazinglands Research Facility near El Reno, OK.

3.1. Remote sensing data

Both the high temporal resolution remote sensing (GOES) and the high spatial resolution remote sensing data (aircraft) were available during SGP97. The remote sensing survey used in this analysis was conducted several days after a heavy rainfall event ($\sim$ 6 cm) that occurred over the El Reno area on June 28, 1997, day of year (DOY) 179. With a general drying trend following this event, aircraft-based remote sensing observations were flown on DOY 183 over the nominal period of 1030–1100 Central Standard Time. During the aircraft mission, measurements from a nearby Mesonet station gave solar radiation $\approx$ 900 W m^{-2} and air temperature of 31 °C under relatively light winds ($\sim$ 2 m s^{-1}). The spatial variability in surface soil moisture conditions and surface temperature in the region was relatively high on this day due to rapid drying of the bare soil/winter wheat fields (French, Schmugge, & Kustas, 2000a; Norman et al., submitted for publication).

3.2. High temporal resolution data

GOES observations of radiative surface temperatures are available every 30 min at $\sim$ 5-km spatial resolution. These surface temperatures were used with early-morning soundings, on-site estimates of canopy characteristics, and surface-station observations of wind speed to estimate surface

Table 2
Radiometric temperature statistical results between subpixel estimates of T_R at 192- and 24-m resolution (i.e., $\hat{T}_{R192}$ and $\hat{T}_{R24}$) using DisTrad and UniTrad versus observed values, namely, T_{R192} and T_{R24} for the four cases described in the text

Case	DisTrad			UniTrad		
	RMSE[a] (C)	R^2	RMSE/σ	RMSE (C)	R^2	RMSE/σ
1	1.61	0.63	0.61	2.26	0.26	0.86
2	1.35	0.74	0.51	1.61	0.48	0.61
3	2.07	0.63	0.62	2.07	0.62	0.62
4	1.84	0.70	0.55	1.64	0.76	0.49

[a] Equation for computing RMSE:

$$\mathrm{RMSE} = \sqrt{\frac{\sum_{i=1}^{n}(M_i - O_i)^2}{n}}$$

where M_i = modeled T_R and O_i = observed T_R.

energy fluxes using ALEXI. Details of implementing GOES with ALEXI and DisALEXI are given in Mecikalski et al. (1999) and Norman et al. (submitted for publication), respectively.

3.3. High spatial resolution data

High-resolution radiometric surface temperature came from the airborne Thermal Infrared Multispectral Scanner

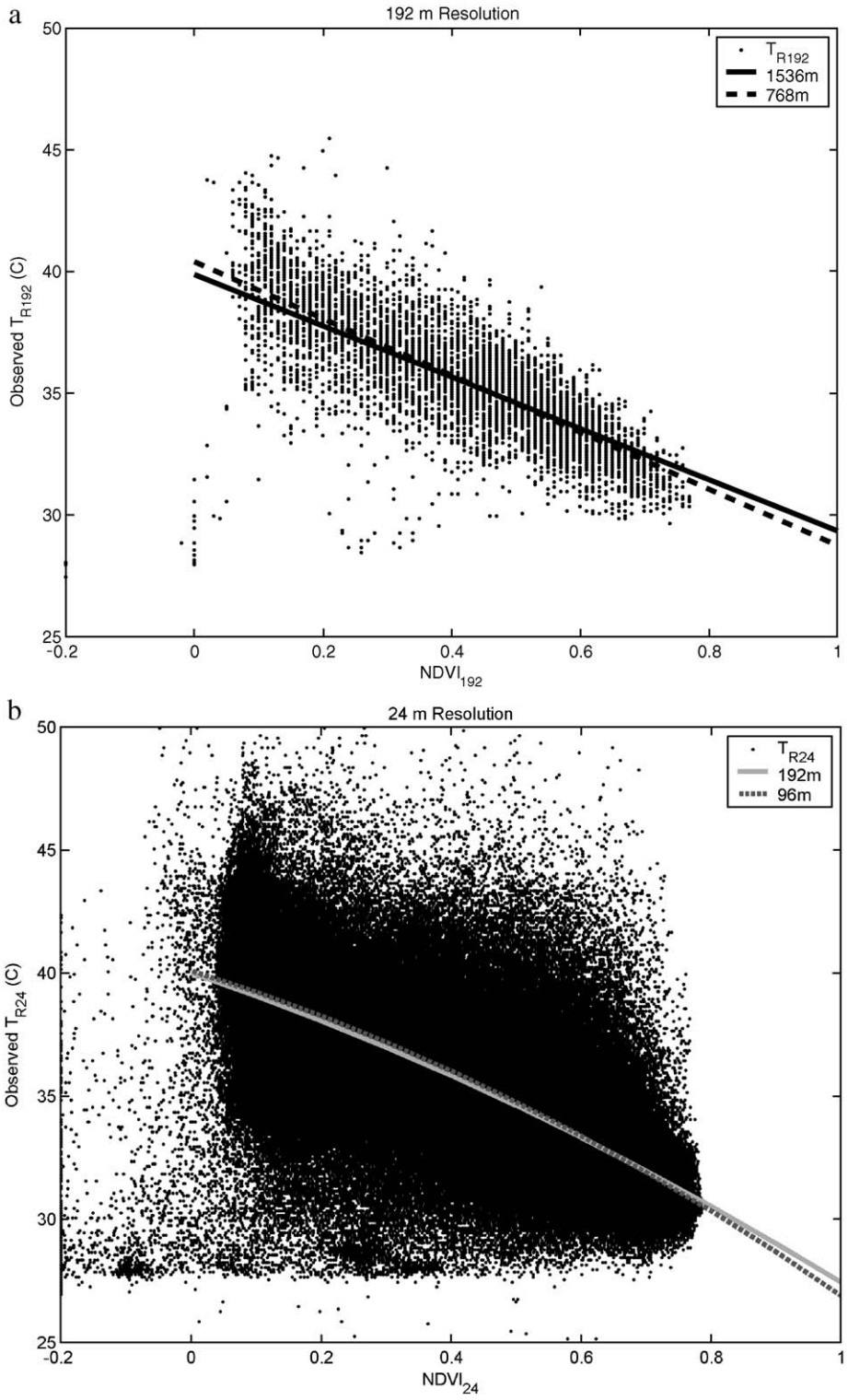

Fig. 1. (a) The NDVI–T_R relationship at 192-m pixel resolution with Eq. (1) fit to the 768- and 1536-m pixel resolution data. (b) The NDVI–T_R relationship at 24-m pixel resolution with Eq. (1) fit to the 192- and 96-m pixel resolution data. (c) A plot of the NDVI–T_R relationship at 96-m pixel resolution. In comparison to (b) at 24-pixel resolution, there is a noticeable reduction in scatter between NDVI and T_R.

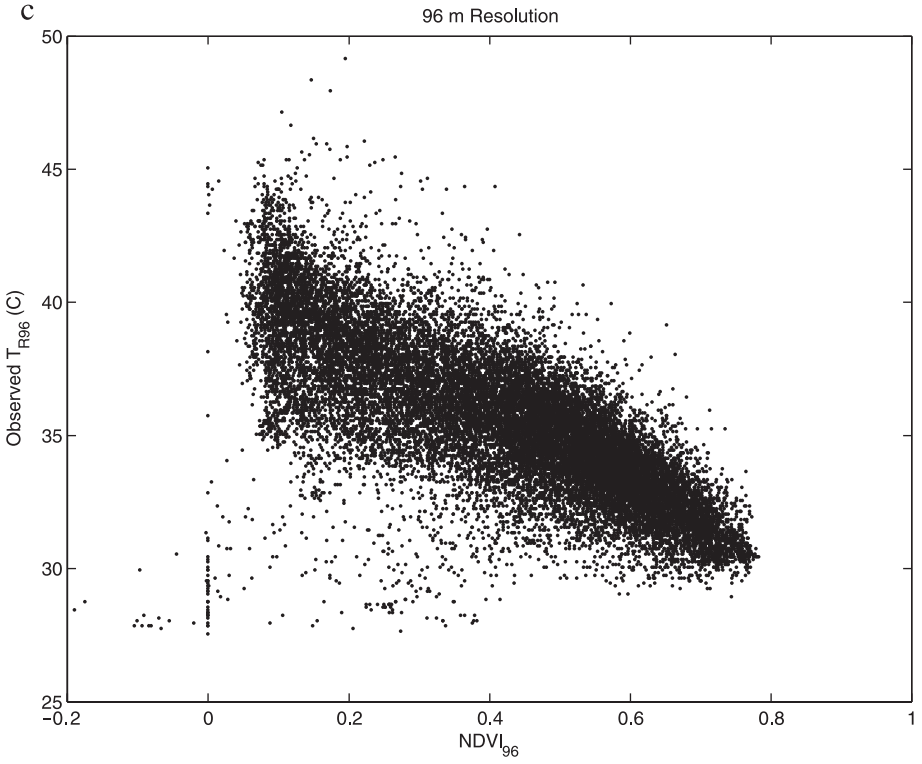

Fig. 1 (*continued*).

(TIMS), while visible–near infrared imagery from the Thematic Mapper Simulator (TMS) was used to create an NDVI and land use map for the region (French et al., 2000a). The TIMS instrument (Palluconi & Meeks, 1985) is a six-channel scanner operating in the thermal infrared (8 to 12 μm) region of the electromagnetic spectrum, while TMS mimics the Landsat TM visible and near-infrared bands. Both sensors were flown on a DOE Cessna Citation aircraft at ~ 5 km agl, which provided radiometric surface temperature and NDVI at 12-m pixel resolution. The El Reno flight lines provided coverage of an area approximately 8 km north–south by 28 km east–west with actual data acquisition time taking less than 5 min. French et al. (2000a,b) provide further details concerning the processing of these data, including correction for emissivity and atmospheric effects. The 12-m TIMS and TMS data were aggregated to 24 m to reduce misregistration errors between the two sensors. This spatial averaging also reduced variability in surface temperature caused by temporal fluctuations inherent in radiometric surface temperature measurements since the magnitude of these fluctuations is attenuated with pixel aggregation (Seguin et al., 1999). To simulate as closely as possible how sensors integrate component radiances from a composite scene at coarser pixel resolutions, aggregation was performed with radiances in the different wavebands. The 24-m radiance data were then further aggregated to 96, 192, 768, and 1536 m, serving as proxies for real observations at these lower resolutions.

4. Results and discussion

4.1. Radiometric surface temperature estimation

The root mean square error (RMSE) statistic (Willmott, 1982), defined in Table 2, was used to assess the level of agreement between observed and estimated T_R using the DisTrad procedure. In addition, the ratio of RMSE to the standard deviations of the observations, σ, (RMSE/σ) was computed, which provides a relative measure of model performance. A value of RMSE/σ ~ 1 indicates poor agreement between model predictions and observations, whereas RMSE/$\sigma \lesssim 0.5$ suggests the scheme is capable of estimating values in satisfactory agreement with observations. With certain assumptions concerning the statistical distributions of the variables, the RMSE/σ ratio is related to the coefficient of determination, R^2, namely, $\sim 1 - R^2$ (Snedecor & Cochran, 1980); since widely used, the R^2 statistic is also reported.

In addition, to gain better insight into the utility of the DisTrad approach, comparison is also made with the "control case" where all NDVI subpixels, NDVI(i), comprising the coarser resolution T_R pixel have the same T_R value. In other words, Eq. (3) is reduced to

$$\hat{T}_{R24}(i) = T_{R96} \tag{4}$$

This will be called the UniTrad approach, which assumes a uniform subpixel T_R field (i.e., all 24-m pixel T_R values

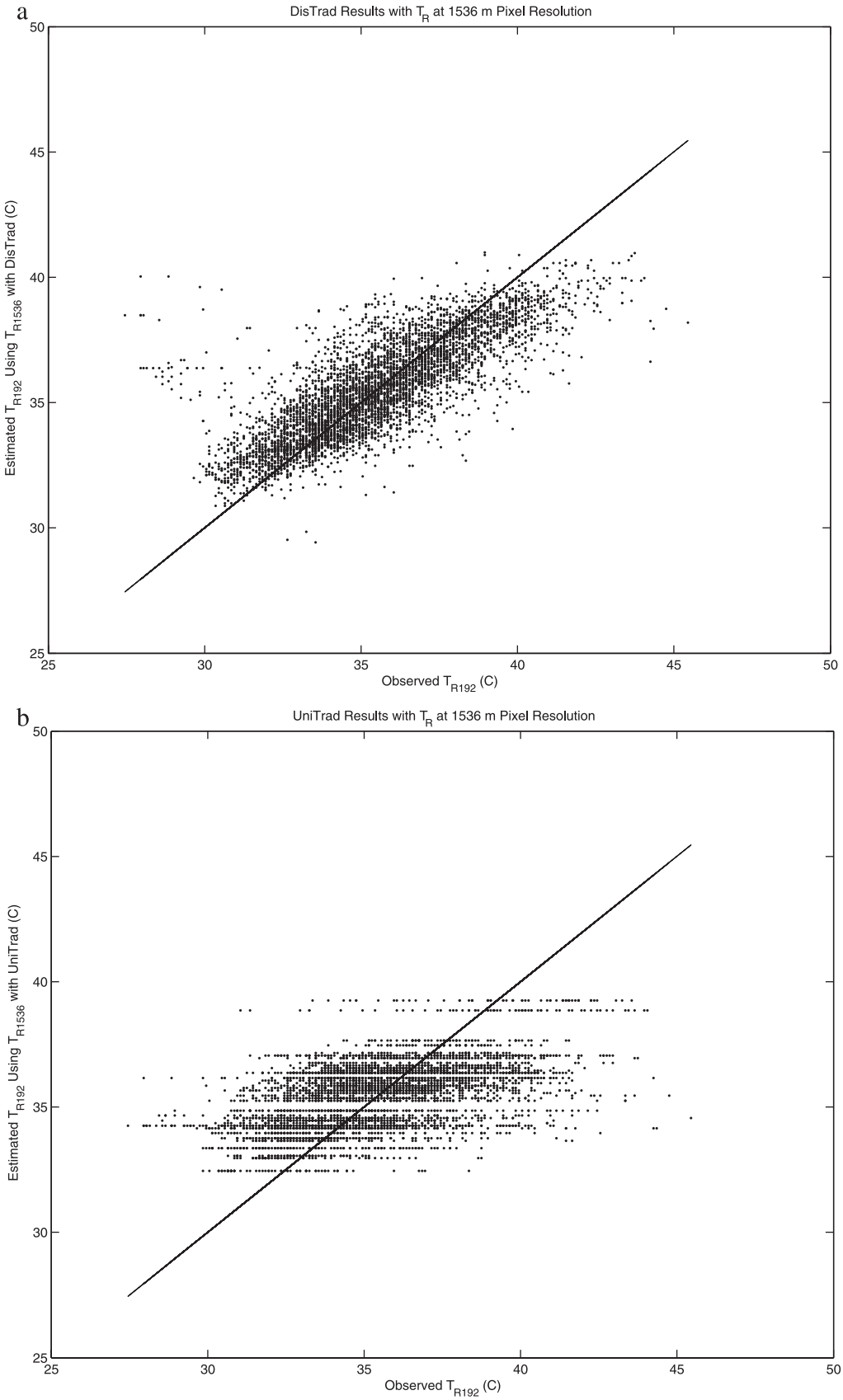

Fig. 2. (a) $\hat{T}_{R192}$ from DisTrad applied to T_{R1536} data versus observed T_{R192}. (b) $\hat{T}_{R192}$ from UniTrad applied to T_{R1536} data versus observed T_{R192}. (c) $\hat{T}_{R24}$ from DisTrad applied to T_{R96} data versus observed T_{R24}, and (d) $\hat{T}_{R24}$ from UniTrad applied to T_{R96} data versus observed T_{R24}. Line indicates perfect agreement.

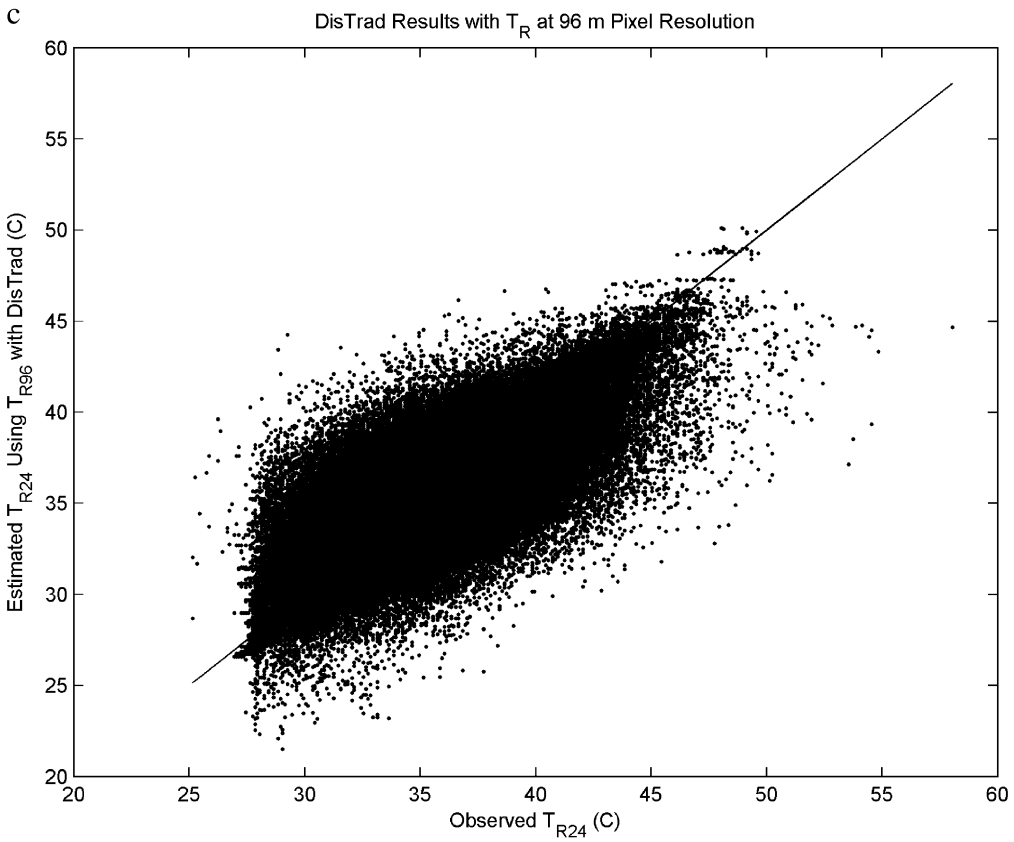

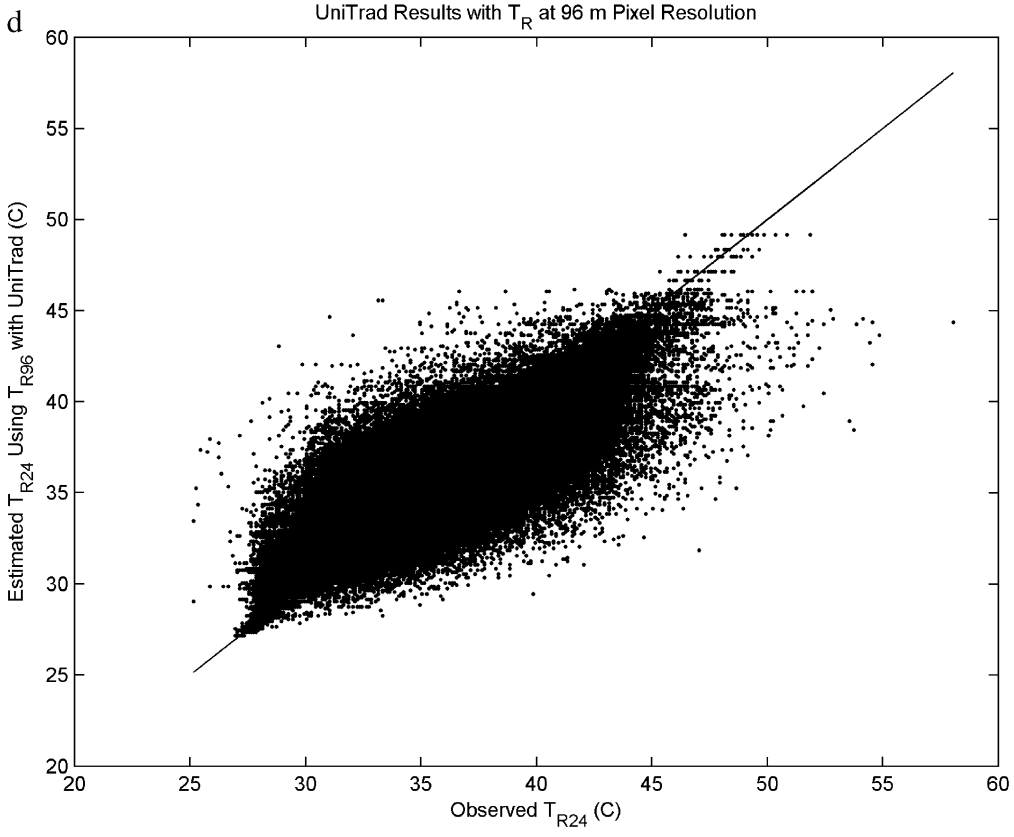

Fig. 2 (*continued*).

estimated from Eq. (4) are equal to the observed 96-m T_R value).

As mentioned earlier, UniTrad and DisTrad are applied to the following cases:

Case 1 Disaggregate T_R from 1536-m pixel resolution to 192 m.
Case 2 Disaggregate T_R from 768-m pixel resolution to 192 m.
Case 3 Disaggregate T_R from 192-m pixel resolution to 24 m.
Case 4 Disaggregate T_R from 96-m pixel resolution to 24 m.

Cases 1 and 2 bracket T_R pixel resolutions of MODIS and AVHRR ($\sim$ 1 km) and apply DisTrad to estimate T_R at the resolution of MODIS-derived NDVI product (250 m). Cases 3 and 4 apply DisTrad at the Landsat 5 (120 m), ASTER (90 m), and Landsat 7 (60 m) T_R pixel resolutions to estimate T_R at the resolution of Landsat and ASTER-derived NDVI product of 30- and 15-m pixel resolution, respectively.

The curves resulting from application of Eq. (1) for cases 1–2 and 3–4 are illustrated in Fig. 1a and b, respectively, overlaid on a pixel-by-pixel comparison of NDVI and T_R at the base resolutions (i.e., 24 and 192 m). The linear form of Eq. (1) was more suitable for cases 1 and 2, while the quadratic equation gave the lowest error for cases 3 and 4. Most of the outliers in the T_R–NDVI space for the 192-m resolution data are pixels containing a significant fraction of water, which have NDVI$\lesssim$0. For the 24-m resolution data, there is considerably more scatter with outliers covering the full range in T_R–NDVI space; hence, the T_R–NDVI relationship is not well defined. Note that the curves generated using Eq. (1) when applied to the coarser resolution data for cases 1 and 2 (Fig. 1a) and cases 3 and 4 (Fig. 1b) are very similar, indicating that pixel resolution did not significantly affect the DisTrad procedure.

The scatter is greatly reduced at 96-m resolution (Fig. 1c), thus obtaining a reasonable regression equation via Eq. (1). The large reduction in scatter in T_R–NDVI space from 24- to 96-m resolution is probably due to differences in the length scales of variability in surface moisture, vegetative cover, and land use, although the attenuation of temporal fluctuations in T_R through the spatial averaging may also be contributing (Seguin et al., 1999). However, at pixel resolutions >10 m, observations (Lagouarde, Duberton, & Moreau, 1997; Seguin et al., 1999) indicate that temporal fluctuations in T_R are relatively minor (i.e., 2 °C $\lesssim$ over a 2–10 min period) and change little with aggregation to coarser resolutions. With the airborne T_R data being used in this analysis having pixel resolutions >20 m, and acquired in less than 5 min, the attenuation in temporal fluctuations in T_R with coarser resolution data is not a major contributing factor to the reduced scatter in T_R–NDVI space observed in aggregation from 24 to 96 m.

In Table 2, the statistical results for DisTrad versus UniTrad approach indicates that the DisTrad procedure is effective in providing disaggregated surface temperatures for cases 1 and 2, the MODIS resolutions, but not any improvement over UniTrad approach at the Landsat/ASTER resolutions. A comparison of $\hat{T}_{R192}$ and $\hat{T}_{R24}$ from DisTrad and UniTrad procedures applied to cases 1 and 4 versus observed T_R illustrates the performance of the two approaches at the lowest and highest resolution conditions (Fig. 2). For case 1 (Fig. 2a and b), DisTrad significantly outperforms UniTrad approach in capturing the spatial variability in T_R at $\sim$ 200 m with the coarser resolution data. On the other hand, for case 4 (Fig. 2c and d), there is no clear advantage in using DisTrad over UniTrad; in fact, the figures suggest that UniTrad actually does slightly better in estimating $\sim$ 25 m T_R.

These results are consistent with the spatial scaling analysis of French (2001) who showed that spatial variance in T_R remains relatively high for pixel resolutions $\lesssim 10^1$ m, while a dramatic decrease in the spatial variance in T_R and in the ability to define field boundaries in this same image occurs at pixel resolutions $\gtrsim$200–400 m. Therefore, UniTrad is bound to perform poorly when applied to T_R pixel resolutions $\gtrsim$400 while gives results similar to DisTrad at resolutions $\lesssim 10^1$ m. This 200–400 m length scale or resolution turns out to be the typical field size, which for this region was either grassland with leaf area index (LAI) generally ranging from $\sim$ 2 to 4 or harvested winter wheat stubble/tilled bare soil with LAI $\sim$ 0. These are highly contrasting surface conditions both in vegetation cover and in T_R (French et al., 2000a, 2000b).

Table 3
Surface energy balance statistical results between using subpixel estimates of T_R at 192- and 24-m resolution (i.e., $\hat{T}_{R192}$ and $\hat{T}_{R24}$) from DisTrad and UniTrad versus using observed values (i.e., T_{R192} and T_{R24}) in DisALEXI for the four cases described in the text

Case/flux	DisTrad			UniTrad		
	RMSE (W m^{-2})	R^2	RMSE/σ	RMSE (W m^{-2})	R^2	RMSE/σ
1/Rn	10	0.43	0.83	13	0.03	1.08
2/Rn	8	0.59	0.67	11	0.25	0.92
3/Rn	12	0.57	0.67	12	0.56	0.67
4/Rn	10	0.66	0.55	9	0.72	0.5
1/*G*	4	0.99	0.12	6	0.98	0.18
2/*G*	3	0.99	0.11	5	0.98	0.15
3/*G*	5	0.99	0.11	5	0.99	0.11
4/*G*	5	0.99	0.11	4	0.99	0.09
1/*H*	24	0.64	0.62	37	0.22	0.95
2/*H*	21	0.72	0.54	31	0.43	0.79
3/*H*	32	0.61	0.64	33	0.57	0.66
4/*H*	28	0.67	0.56	26	0.72	0.52
1/LE	29	0.63	0.41	44	0.59	0.63
2/LE	25	0.87	0.36	36	0.74	0.51
3/LE	38	0.80	0.46	39	0.78	0.47
4/LE	34	0.83	0.41	31	0.86	0.37

4.2. Surface energy balance estimation using DisALEXI

An analysis similar to the subpixel surface temperature retrieval was performed with the surface energy balance output for cases 1–4 using DisALEXI with T_R observations and estimated T_R from DisTrad and UniTrad methods. Values of RMSE, R^2, and the ratio RMSE/σ for the four energy balance components, namely, net radiation (Rn), soil heat flux (G), sensible heat flux (H), and latent heat flux (LE), are listed in Table 3.

The results summarized in Table 3 are similar to the findings with T_R, namely, that there is an advantage in employing the DisTrad procedure for estimating subpixel surface energy fluxes over this landscape at the MODIS/AVHRR T_R and NDVI resolutions (cases 1 and 2). However, there is marginal to essentially no benefit in using DisTrad in comparison to the simple UniTrad technique at the Landsat/ASTER T_R and NDVI resolutions (cases 3 and 4). In addition, the RMSE values for H and LE for cases 3 and 4 with either T_R disaggregation technique start to approach the ~ 50 W m^{-2} model-measurement uncertainty and therefore have marginal benefit in providing reliable within-field (i.e., $\sim 10^1$-m resolution) surface heat flux maps over this particular landscape. Hence, the DisTrad procedure applied to T_R–NDVI data would have the greatest utility for disaggregation of T_R pixels with resolutions >200–400 m. This result is also supported by the flux-scaling work of French (2001) who found that at pixel resolutions aggregated beyond ~ 200 m, errors in the modeled heat fluxes become significant and difficult to relate to heat fluxes at finer resolutions. Below this length scale, the disaggregation of T_R with DisTrad does not show a significant advantage over assuming a uniform subpixel T_R distribution for heat flux calculations.

A final statistical analysis is performed for the turbulent heat fluxes, H and LE, which had the largest RMSE values, by computing and comparing the probability density functions (pdfs) of differences between DisALEXI output using the observed versus estimated T_R under the four cases (i.e., modeled H and LE using the observed or "actual" T_R minus modeled H and LE using T_R derived from DisTrad and UniTrad approaches). Besides the mean and standard deviation, the skewness and kurtosis (third and fourth moments about the mean normalized by σ; see Table 4) of the pdfs are compared to a normal distribution, which has a skewness = 0 and a kurtosis = 3. For cases 1 and 2, the pdfs of H and LE differences are illustrated in Fig. 3, while the pdfs of H and LE differences for cases 3 and 4 are illustrated in Fig. 4 using both the DisTrad and UniTrad approach. The mean, standard deviation, skewness, and kurtosis values for the pdfs are listed in Table 4.

The pdfs of the H and LE differences using DisTrad and UniTrad plotted for cases 1 and 2 (Fig. 3) indicate a significantly narrower distribution using DisTrad compared to UniTrad, while for cases 3 and 4 (Fig. 4), the pdfs look very similar. The mean of the differences or bias is small for all four cases with values ± 5 W m^{-2}. The σ values in Table 4 are essentially the same as the RMSE values listed in Table 3, indicating generally a lower variance in the heat flux differences using DisTrad compared to UniTrad. The skewness values using DisTrad range between ± 2 (see Table 4),

Table 4
Mean, standard deviation, skewness and kurtosis of H and LE differences between using observed values (i.e., T_{R192} and T_{R24}) versus subpixel estimates of T_R at 192- and 24-m resolution (i.e., $\hat{T}_{R192}$ and $\hat{T}_{R24}$) from DisTrad and UniTrad procedures in DisALEXI for the four cases described in the text

Case/flux	DisTrad				UniTrad			
	Mean (W m^{-2})	Standard deviation (W m^{-2})	Skewness[a] (−)	Kurtosis[b] (−)	Mean (W m^{-2})	Standard deviation (W m^{-2})	Skewness (−)	Kurtosis (−)
1/H	3	24	−1.03	12.5	−5	37	−0.95	7.6
2/H	~0	21	−1.36	21.3	−3	31	−0.85	8.1
3/H	3	31	1.66	21.4	1	33	0.44	15.7
4/H	2	29	1.92	25.6	1	26	0.88	24.9
1/LE	−3	29	1.03	12.3	3	44	0.56	6.3
2/LE	~0	25	1.46	21.6	2	36	0.50	7.1
3/LE	−3	38	−1.18	16.1	−2	39	−0.43	12.3
4/LE	−2	34	−1.39	19.1	−2	31	−0.73	18.9

[a] Equation for computing skewness of variable X with mean, $\bar{X}$:

$$\text{skewness} = \frac{\sum_{i=1}^{n}(X_i - \bar{X})^3}{\frac{n}{\sigma^3}}.$$

[b] Equation for computing kurtosis of variable X with mean, $\bar{X}$:

$$\text{kurtosis} = \frac{\sum_{i=1}^{n}(X_i - \bar{X})^4}{\frac{n}{\sigma^4}}.$$

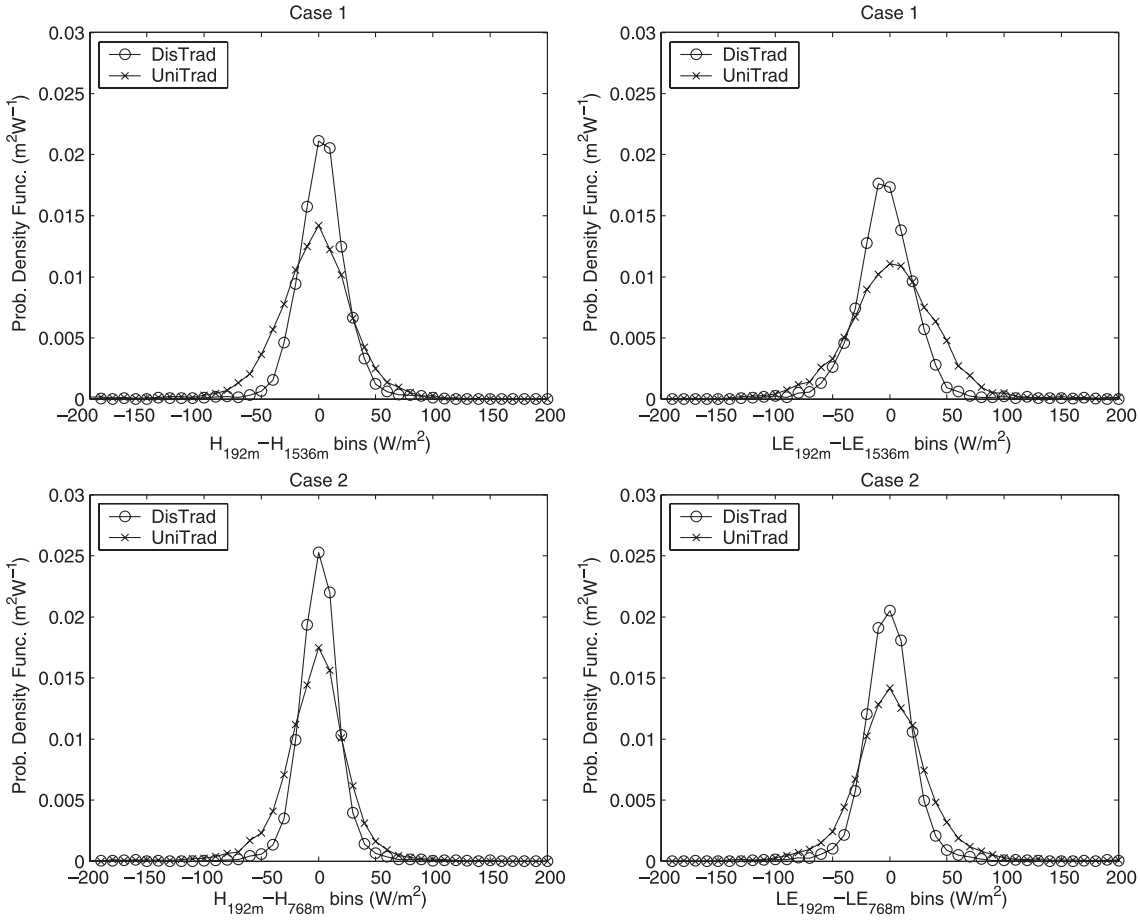

Fig. 3. The pdfs of the differences in H and LE for cases 1 and 2, where $\hat{T}_{R192}$ from DisTrad and UniTrad is used in DisALEXI and contrasted to using observed, T_{R192}, in computing the heat fluxes with DisALEXI.

whereas the kurtosis departs significantly from the value from a normal distribution (i.e., kurtosis = 3) ranging instead between 10 and 25. The large kurtosis values using DisTrad, with most ~ 20, indicates a very narrow distribution, and as can be seen from Figs. 3 and 4, these differences in H and LE primarily fall within ± 50 W m^{-2}. With UniTrad, the skewness values are closer to a normal distribution with a range of ± 1. The kurtosis values indicate a narrower than normal distribution, but the values are less than 10 for cases 1 and 2 and are even slightly lower than the kurtosis values associated with DisTrad for cases 3 and 4.

In summary, the pdfs of H and LE differences using DisTrad for estimating T_R versus using observed T_R are generally narrower (i.e., higher kurtosis values) than with the UniTrad approach, particularly for cases 1 and 2 (see Fig. 3). This, together with the statistical results summarized in Tables 2–4, suggest that for cases 1 and 2, the DisTrad procedure provides markedly better estimates of subpixel T_R values compared to the UniTrad approach, while there is little, if any, improvement for cases 3 and 4. In addition, the higher skewness in the pdfs using DisTrad compared to UniTrad suggests that more asymmetry exists in the DisTrad distributions. More asymmetry, but a small bias (Table 4), in the heat flux differences using DisTrad versus UniTrad indicates that a greater number of modeled fluxes with estimated subpixel T_R values from DisTrad differ significantly, being either markedly higher or lower than values computed with actual T_R.

For H differences (i.e., modeled H using the observed T_R minus modeled H using T_R derived from DisTrad and UniTrad approaches), the skewness is <0 using either the DisTrad and UniTrad approach for cases 1 and 2, whereas the opposite holds true (i.e., skewness>0) for cases 3 and 4. This result must be indicative of the relative influence of the warm and cool patches at the two base pixel resolutions, namely, ~ 200 and ~ 25 m. In disaggregation of T_R from ~ 1000 to ~ 200 m (cases 1 and 2), the negative skewness for H differences suggests that the disaggregation procedures are unable to detect cooler subpixel patches. The opposite appears to hold true in disaggregation of T_R from ~ 100 to ~ 25 m (cases 3 and 4); the positive skewness for H differences suggests that there are warmer subpixel patches not being detected by the disaggregation procedures.

These results appear to be in qualitative agreement with French (2001). He found that at pixel resolutions ≳200–400 m, T_R and NDVI data are a composite of warmer bare soil and cooler vegetated fields. Consequently, the disag-

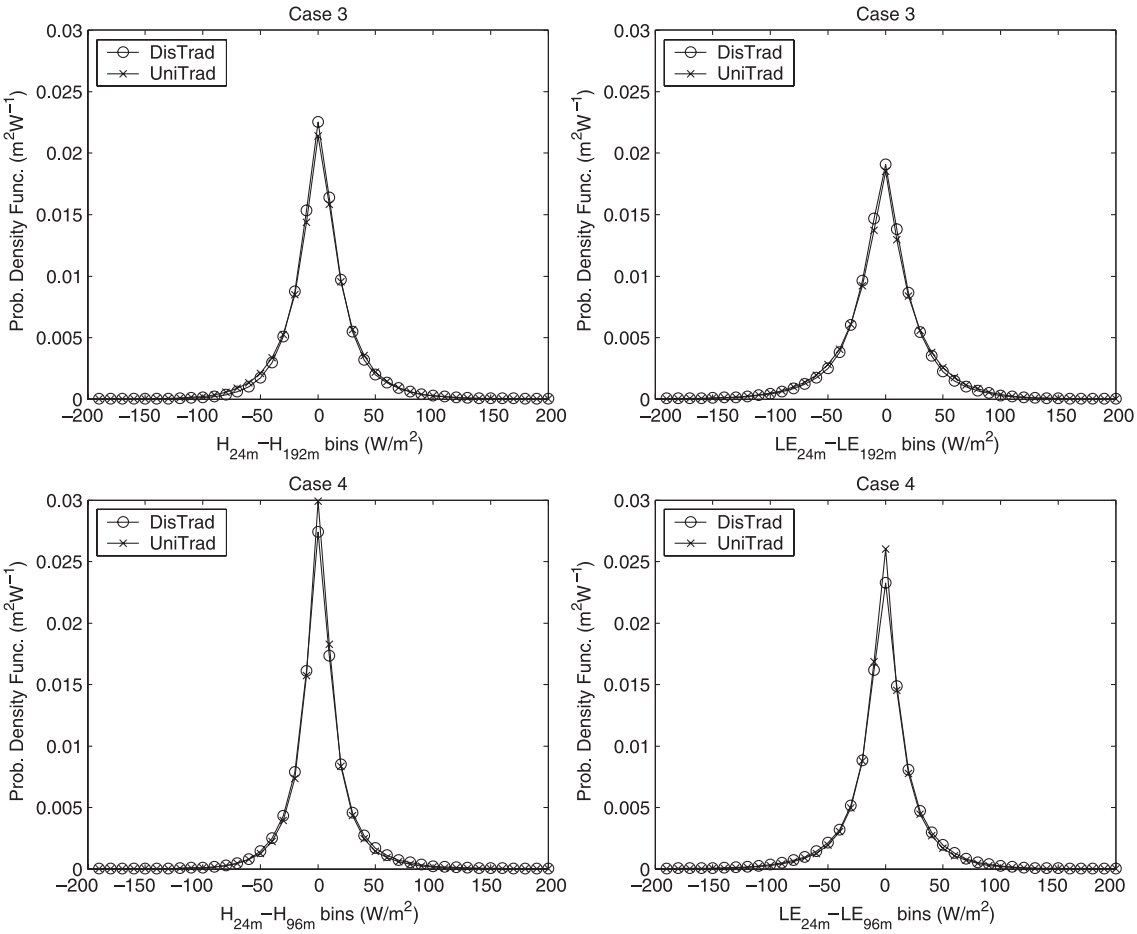

Fig. 4. The pdfs of the differences in H and LE for cases 3 and 4, where $\hat{T}_{R24}$ from DisTrad and UniTrad is used in DisALEXI and contrasted to using observed, T_{R24}, in computing the heat fluxes with DisALEX.

gregation of T_R from these mixed pixels has a tendency to overestimate subpixel T_R values for some of the cooler patches in the image. On the other hand, below this threshold pixel resolution, French (2001) found that field boundary discrimination is preserved, and hence the warmer and cooler patches are more closely associated with the low cover/bare soil and vegetated fields, respectively. However, within these field boundaries, French (2001) still found significant variations in T_R due to variability in vegetation cover and surface moisture conditions. For the particular scene analyzed here, it appears that the disaggregation procedures have a tendency to underestimate subpixel T_R values for some of the warmer patches in the image.

5. Conclusions

A procedure for disaggregating radiometric surface temperature T_R (i.e., DisTrad approach) in order to derive a subpixel distribution at ~ 25- and ~ 200-m resolution is evaluated using airborne imagery collected over the Southern Great Plains. The estimated surface temperatures at these two resolutions are similar to NDVI pixel resolutions from MODIS and ASTER/Landsat satellite sensors.

The comparisons with actual T_R data indicate that DisTrad can provide subpixel T_R values at the MODIS NDVI pixel resolution within ~ 1.5 °C uncertainty, but at the ASTER/Landsat NDVI resolution, subpixel estimates from DisTrad are not any more reliable than assuming a uniform subpixel T_R field (i.e., UniTrad method). This result is consistent with an independent spatial scaling study showing that the greatest loss of T_R spatial variability came at pixel resolutions ≳200–400 m, the typical dimension of the agricultural field boundaries (French, 2001).

The estimated and observed T_R values were used with the Disaggregated Atmosphere Land Exchange Inverse (DisALEXI) model for estimating heat fluxes. Comparisons of model output using DisTrad and UniTrad estimates of T_R with actual or observed T_R also indicated that the utility of DisTrad is greatest at the MODIS NDVI resolution. The errors, as quantified by RMSE, in sensible and latent heat flux computations using disaggregated versus observed surface temperatures range from 20 to 30 W m^{-2}. These errors are well within typical uncertainty in modeled and measured heat fluxes reported to be ~ 50 W m^{-2} (Twine et al., 2000).

Although these preliminary results pertain strictly to the landscape and environmental conditions that existed in this region, much of the Southern Great Plains has agricultural field dimensions similar to this experimental site, and, consequently, this disaggregation procedure could be applied regionally for estimating field scale ET. In fact, based on the results of Townshend and Justice (1988), application of DisTrad to 1-km resolution T_R to achieve MODIS NDVI resolution (250 m) T_R could provide significantly more detailed information concerning the impact of land transformations on the surface energy balance and ET. With the use of MODIS combined with GOES, and the DisTrad and DisALEXI modeling schemes, there is much greater potential for routine ET monitoring at the 10^2-m resolution than with ASTER or Landsat because of the frequency of GOES and MODIS coverage. Future work will involve testing this disaggregation procedure in concert with DisALEXI using satellite data collected over a variety of landscapes and under a range of environmental conditions.

Acknowledgements

This work was supported by the NASA EOS and Land Surface Hydrology Programs. We are indebted to Dr. Tom Jackson for organizing and coordinating The Southern Great Plains 1997 Hydrology Experiment and Dr. Ming Ying Wei of NASA Headquarters whose guidance and support made this project of greater value than its individual components. Comments of the reviewers were helpful in clarifying factors contributing to the spatial–temporal variability in radiometric surface temperature.

References

Anderson, M. C., Norman, J. M., Diak, G. R., Kustas, W. P., & Mecikalski, J. R. (1997). A two-source timt-integrated model for estimating surface fluxes using thermal infrared remote sensing. *Remote Sensing of Environment*, *60*, 195–216.

Brock, F. V., Crawford, K. C., Elliott, R. L., Cuperus, G. W., Stadler, S.J., Johnson, H. L., & Eilts, M. D. (1995). The Oklahoma Mesonet, a technical overview. *Journal of Atmospheric and Oceanic Technology*, *12*, 5–19.

Carlson, T. N., Gillies, R. R., & Perry, E. M. (1994). A method to make use of thermal infrared temperature and NDVI measurements to infer soil water content and fractional vegetation cover. *Remote Sensing Reviews*, *52*, 45–59.

French, A. N. (2001). Scaling of surface energy fluxes using remotely sensed data. PhD Dissertation, University of Maryland.

French, A. N., Schmugge, T. J., & Kustas, W. P. (2000a). Surface fluxes over the SGP site with remotely sensed data. *Physics and Chemistry of the Earth, Part B*, *25*, 167–172.

French, A. N., Schmugge, T. J., & Kustas, W. P. (2000b). Discrimination of senescent vegetation using thermal emissivity contrast. *Remote Sensing of Environment*, *74*, 249–254.

French, A. N., Schmugge, T. J., & Kustas, W. P. (2002). Estimating evapotranspiration over El Reno, Oklahoma with ASTER imagery. *Agronomie*, *22*, 106.

Gillies, R. R., & Carlson, T. N. (1995). Thermal remote sensing of surface soil water content with partial vegetation cover for incorporation into climate models. *Journal of Applied Meteorology*, *34*, 745–756.

Jackson, T. J., Le Vine, D. M., Hsu, A. Y., Oldak, A., Starks, P. J., Swift, C. T., Isham, J. D., & Haken, M. (1999). Soil moisture mapping at regional scales using microwave radiometry: the Southern Great Plains hydrology experiment. *IEEE Transactions on Geoscience and Remote Sensing*, *37*, 2136–2151.

Kustas, W. P., & Norman, J. M. (1996). Use of remote sensing for evapotranspiration monitoring over land surfaces. *Hydrological Sciences Journal*, *41*, 495–516.

Kustas, W. P., & Norman, J. M. (1999). Evaluation of soil and vegetation heat flux predictions using a simple two-source model with radiometric temperatures for partial canopy cover. *Agricultural and Forest Meteorology*, *94*, 13–25.

Lagouarde, J. P., Duberton, S., & Moreau, P. (1997). Analyse de l'erodicité de la température de surface sur des couverts forestiers á diverses résolutions spatiales. In G. Guyot, & T. Phulpin (Eds.), *Proc. physical measurements and signatures in remote sensing* (pp. 303–310). Rotterdam: Balkema.

Mecikalski, J. R., Diak, G. R., Anderson, M. C., & Norman, J. M. (1999). Estimating fluxes on continental scales using remotely-sensed data in an atmospheric-land exchange model. *Journal of Applied Meteorology*, *38*, 1352–1369.

Moran, M. S., Clarke, T. R., Inoue, Y., & Vidal, A. (1994). Estimating crop water deficit using the relation between surface–air temperature and spectral vegetation index. *Remote Sensing of Environment*, *49*, 246–263.

Moran, M. S., Rahman, A. F., Washburne, J. C., Goodrich, D. C., Weltz, M. A., & Kustas, W. P. (1996). Combining the Penman–Monteith equation with measurements of surface temperature and reflectance to estimate evaporation rates from semiarid grassland. *Agricultural and Forest Meteorology*, *80*, 87–109.

Norman, J. M., Kustas, W. P., & Humes, K. S. (1995). A two-source approach for estimating soil and vegetation energy fluxes from observations of directional radiometric surface temperature. *Agricultural and Forest Meteorology*, *77*, 263–293.

Norman, J. M., Anderson, M. C., Kustas, W. P., French, A. N., Mecikalski, J., Torn, R., Diak, G. R., Schmugge, T. J., & Tanner, B. C. W. (2003). Remote-sensing of surface energy fluxes at 10′ -m pixel resolutions. *Water Resources Research* (submitted for publication).

Palluconi, F. D., & Meeks, G. R. (1985). Thermal infrared multispectral scanner (TIMS): an investigator's guide to TIMS data. JPL Publication 85_32, Jet Propulsion Laboratory, California Institute of Technology, Pasadena, California.

Price, J. C. (1990). Using spatial context in satellite data to infer regional scale evapotranspiration. *IEEE Transactions on Geoscience and Remote Sensing*, *GE-28*, 940–948.

Seguin, B., Becker, F., Phulpin, T., Gu, X. F., Guyot, G., Kerr, Y., King, C., Lagouarde, J. P., Ottle, C., Stoll, M. P., Tabbagh, A., & Vidal, A. (1999). IRSUTE: a minisatellite project for land surface heat flux estimation from field to regional scale. *Remote Sensing of Environment*, *68*, 357–369.

Seguin, B., Lagouarde, J. -P., & Saranc, M. (1991). The assessment of regional crop water conditions from meteorological satellite thermal infrared data. *Remote Sensing of Environment*, *35*, 141–148.

Snedecor, G. W., & Cochran, W. G. (1980). *Statistical methods*. Ames, Iowa USA: The Iowa Sate University Press. 507 pp.

Shafer, M. A., Fiebrich, C. A., Arndt, D. S., Fredrickson, S. E., & Hughs, T. W. (2000). Quality assurance procedures in the Oklahoma mesonetwork. *Journal of Atmospheric and Oceanic Technology*, *17*, 474–494.

Townshend, J. G. R., & Justice, C. O. (1988). Selecting the spatial resolution of satellite sensors required for global monitoring of land transformations. *International Journal of Remote Sensing*, *9*(2), 187–236.

Twine, T. E., Kustas, W. P., Norman, J. M., Cook, D. R., Houser, P. R., Meyers, T. P., Prueger, J. H., Starks, P. J., & Wesely, M. L. (2000). Correcting eddy-covariance flux underestimates over a grassland. *Agricultural and Forest Meteorology*, *103*, 279–300.

Willmott, C. J. (1982). Some comments on the evaluation of model performance. *Bulletin of the American Meteorological Society*, *11*, 1309–1313.